Intrinsic heterogeneity of grain boundary states in ultrafine-grained Ni: A cross-scale study by SIMS and radiotracer analyses

L.T. Belkacemi, M. Vaidya, S. Sevlikar, A. Hassanpour, F. Jomard, D. Irmer, C. Guerre, L. Martinelli, Cecilie Duhamel, G. Wilde, et al.

Version of Record: https://www.sciencedirect.com/science/article/pii/S2589152922000825
Manuscript_db74456624873af0873c52984c3223ef

Intrinsic heterogeneity of grain boundary states in ultrafine-grained Ni: a cross-scale study by SIMS and radiotracer analyses

L.T. Belkacemi[a,b], M. Vaidya[c,d], A. Hassanpour[c], F. Jomard[e], D. Irmer[a], C. Guerre[f], L. Martinelli[f], C. Duhamel[a], G. Wilde[c], V.A. Esin[a*], S.V. Divinski[c]

[a]*MINES ParisTech, PSL University, Centre des Matériaux (CNRS UMR 7633), Évry, France*

[b]*Department of Microstructure Physics and Alloy Design, Max-Planck-Institut für Eisenforschung, Düsseldorf, Germany*

[c]*Institute of Materials Physics, University of Münster, Germany*

[d]*Indian Institute of Technology Hyderabad, Hyderabad, India*

[e]*Université de Versailles-Saint-Quentin, CNRS UMR 8635, GEMaC, Versailles, France*

[f]*Université Paris-Saclay, CEA, Service de la Corrosion et du Comportement des Matériaux dans leur Environnement, Gif-sur-Yvette, France*

[*]corresponding author (vladimir.esin@mines-paristech.fr)

Abstract.

Using a correlated diffusion study applying secondary-ion mass spectroscopy (SIMS) and radiotracer analyses, the co-existence of both deformation-modified non-relaxed and relaxed high-angle grain boundaries (GBs) in ultrafine-grained Ni of 2N6 purity processed by equal channel angular pressing (ECAP) is clearly revealed. Due to different depth and lateral resolutions and using experimentally accessible diffusion times, SIMS provides a direct access to the properties of relaxed "slow" GBs (at short penetration depths) while the radiotracer measurements reveal simultaneously the contribution of the deformation-modified "fast" GBs (at large penetration depths). The temperature stability of ultrafine-grained structure of 2N6 Ni is investigated using electron back-scatter diffraction after annealing treatments corresponding to the diffusion experiments. No changes of the ECAP-produced microstructure occur at 403 K, while the ultrafine-grained structure is remarkably evolving to a coarse-grained one at 603 K. The knowledge of the microstructure evolution is used to quantify the diffusion data. The combination of the two complementary techniques allows not only to perform a cross-scale analysis of the mass transport, but also to probe consistently the existence and kinetic properties of different multi-level hierarchic microstructure features. Therefore, the results obtained is a step forward in a better understanding of the physics of ultra-fine-grained materials (UFG). For the first time in the case of UFG materials, the SIMS technique is used in a mode with lateral resolution which is correlated with the microstructure

characteristics resolving a multi-level hierarchy of diffusion properties of short circuits in severe plastically deformed materials.

Keywords: Diffusion, ultrafine-grained materials, grain boundaries, EBSD, geometrically necessary dislocations.

1. Introduction

The faster diffusivity of substitutional atoms along the grain boundaries (GBs) than through the crystal lattice has been clearly demonstrated during the last few decades [1–7]. GBs can consequently play the role of atom sources and sinks, which can alter the properties of a polycrystalline material. Indeed, atom mixing and mass transport govern physical phenomena such as phase transformation, high temperature oxidation, recrystallization, grain growth or creep that underpin the manufacturing, joining and ageing of a slew of important technologies [8–10]. These short-circuit diffusion paths were largely studied especially in ultrafine-grained (UFG) materials [11–13] which raised much interest since the first concepts of nanocrystalline materials were proposed [14,15]. The use of severe plastic deformation (SPD) techniques [16] to produce nanostructured materials, such as equal-channel angular pressing (ECAP), as an alternative to nanopowder compaction [17–19], has been intensively increased to enhance their properties [20–24]: reasonable ductility, high strength, toughness, fatigue life and wear resistance [25–28]. As-produced nanomaterials are dense, even though micropores and cracks may also be present [29]. A percolating porosity can enhance the atomic transport especially at low temperatures, as revealed by the radiotracer diffusion measurements [30,31]. For instance, self- and Cu solute GB diffusion in SPD-processed Ni have previously been demonstrated to be significantly enhanced with respect to those in the corresponding coarse-grained materials [32].

The ultra-fast diffusion rates measured in SPD-processed materials were explained by formation of specific GBs exhibiting an increased free energy and significant residual microstrains [33]. These non-relaxed high-angle GBs are called "deformation-modified" GBs [33] in order to avoid previously suggested [34] and ambiguous term “non-equilibrium” interfaces. They have been reported as sinks for lattice dislocations [35] as evidenced by in situ transmission electron microscopy (TEM) [36–38] and lead to the disordering of networks of grain boundary dislocations (GBDs) [34]. These GBs exhibit higher diffusion coefficients of one to several orders of magnitude as well as higher sliding and migration rates than

relaxed GBs [39]. Note that GB migration enhances the total flux of diffusing atoms in a material, as demonstrated by Glaeser and Evans [40]. Therefore, non-relaxed GBs in nanostructured metallic alloys obtained by high-energy deformation processes are suspected to be responsible for a higher GB diffusivity [41].

Radiotracer measurements of Ni GB diffusion in SPD Cu and Cu-based alloys revealed that not all grain boundaries feature "deformation-modified" state. Indeed, a majority of high-angle GBs are characterized by "normal" diffusion rates which are characteristic for well-annealed polycrystalline materials [31,42]. A hierarchy of short-circuit diffusion paths has been suggested [43], with the "deformation-modified" GBs topping the whole spectrum of interfaces. While in ultrafine-grained Cu it was possible to measure the two different diffusion rates in a single radiotracer diffusion experiment [31,42], it was impossible to observe simultaneously these contributions in, e.g., UFG Ni in which several orders of magnitude difference between the diffusion rates has been suggested [32]. Ideally, both short (about 100 nm) and large (significantly above 10 μm) penetration depths have to be simultaneously resolved in a single experiment, which is hardly accessible for any method. The basically different enhancements of diffusion along the deformation-modified GBs with respect to those in coarse-grained counterparts in Cu and Ni are probably explained by the distinctly different homologous temperatures of plastic deformation in these two materials, $0.27T_m$ and $0.20T_m$, respectively (where T_m is melting temperature). Correspondingly, relaxation processes by room-temperature plastic deformation in nickel are significantly retarded with respect to those in copper. Are the slow-diffusing boundaries in ECAP-processed nickel similar to those in coarse-grained polycrystalline material? Their existence has been proven by the previous self-diffusion measurements using the radiotracer technique [32], but the diffusion properties were not quantified.

Furthermore, the determination of the diffusion coefficient of a species should be carried out by taking into account the potential changes occurring in the microstructure (recrystallization, grain growth) during diffusion annealing, as performed in [44,45]. A GB self-diffusion study recently conducted at 423 K using radiotracer technique on two UFG Ni prepared by high-pressure torsion (HPT) and with different purities [46] reported a two-stage penetration (branches I and II) in the profile measured for the 4N Ni while a single-stage penetration was observed for the less pure 2N6 Ni (only branch II). The branch II, at higher depths, exhibiting a lower slope is associated with fast GB diffusion along GBs that did not relax after being modified by the deformation. The steep slope part of the penetration profile (branch I, at

lower depths) is only present in the 4N UFG-Ni material where a pronounced recrystallization took place at 423 K when compared to the less pure 2N6 Ni (no recrystallization). This branch is attributed to the recrystallization front that separates the recrystallized areas from the remaining UFG areas as well as to relaxed high-angle GBs which contribute to a negligible extent to the total diffusion flux [46]. The reason for such difference in microstructure evolutions in the 4N and 2N6 UFG-Ni, investigated further in [47], put forward the role of impurities in the slowdown of the recrystallization front, causing the survival of the remaining UFG areas which act as ultrafast diffusion paths. In that case, penetration profiles obtained during diffusion experiments revealed critical information on existing and newly formed interfaces and microstructural features, suggesting the possibility for diffusion experiments to be considered as a valuable tool to investigate the microstructure evolution under sufficiently high temperature.

The previously reported results on UFG Ni were obtained using the radiotracer technique, which is the standard method for studying self- and solute diffusion in solids [48]. This method enables one to detect tiny concentrations of diffusion species, being much smaller than the ones detected through other means (chemical, gravimetric, dimensional analyses). The mechanical sectioning employed during radiotracer analysis limits the profile depth resolution, thereby setting a lower limit on the diffusion distances, i.e. on the diffusion temperatures. If one uses ion-beam sputtering, nanometer-large penetration depths can be measured, while deep tracer penetration still remains unresolved.

The second technique, widely used to trace impurities in materials is the secondary-ion mass spectrometry (SIMS). Here, non-radioactive tracers can be deposited. The popularity of SIMS also stems from its ability to identify elements with a spatial resolution of tens of micrometers and a depth resolution of few nm. Therefore, this method enables to collect an impurity signal over short distances with a good accuracy, making thereby possible the measurement of diffusion coefficients obtained at low temperatures.

In this work, both radiotracer and SIMS techniques are combined to study Cr diffusion in UFG nickel at low temperatures ranging from 403 to 603 K and trace the whole spectrum of possible GB diffusion rates. For a first time, a co-existence of relaxed and deformation-modified grain boundaries in UFG Ni is directly resolved, their basic diffusion properties are quantified and the relaxation of GB-induced state of interfaces is traced in detail. Such microstructure features in UFG Ni were anticipated in the previous studies available in the

literature but no direct experimental evidence has ever been provided. The reason was the application of a single technique in one investigation that is intrinsically limited with respect to the range of the diffusion coefficients which could be simultaneously measured at the given temperature using accessible diffusion times (ranging commonly from minutes to months). A combination of two complementary techniques with different ranges of accessible diffusion coefficients, viz. radiotracer and SIMS, allowed to solve the problem. Therefore, the results obtained is a step forward in a better understanding of the physics of ultra-fine-grained materials. Moreover, for the first time in the case of UFG materials, the SIMS technique is used in a mode with lateral resolution which is correlated with the microstructure characteristics. A solution regarding the uncertainties related to the lateral resolution in SIMS is applied. Indeed, one should consider the sensitivity reached by SIMS which is proportional to the amount of sputtered material (within acceptable scan times), but also gets worsened as the probe size is reduced. Here, by selecting the area of interest with still a sufficient signal (sensitivity), we could be able to investigate the microstructural features on the extreme surface that could have never been looked into up to now due to experimental artefacts. This methodology gives access to the investigation of microstructural features/defects right below the surface, which was previously not possible, and thereby brings new insights into the use of this technique, as a way to analyze the chemical composition but also the type of microstructural features.

Cr is chosen as a suitable element to trace GB diffusion properties of pure Ni using SIMS. Hypothetically, one may use highly enriched ^{64}Ni isotope to probe Ni self-diffusion and not be biased by any segregation tendency of the diffusing element. However, the background signal would be too high due to the natural abundance of ^{64}Ni, about 1%. Note that this level is small enough to enable measurements of volume diffusion, but it is too high to facilitate grain boundary diffusion measurements. Hence, heterodiffusion had to be considered and, in order to limit the effect of the solute on grain boundaries, this has to be a non-segregating solute. Chromium appeared as the ideal element. Indeed, as being a non-segregating element, the analysis of diffusion results was quite straightforward and the microstructure features in UFG Ni were easily revealed. In the case of segregating species, like Ag, the analysis would have been biased and much more complex since a number of non-linear effects and different segregation structures (or complexions) could be expected. Moreover, we can emphasize that a study of diffusion of not segregating solute is a mandatory stage before taking into consideration a strong segregating solute. The case of strongly segregating solute is still open

and can now be studied thanks to the contribution of our current results. The activation energy of GB diffusion of Cr in Ni is known to be lower than that of lattice diffusion. The first values were reported by Pruthi et al. [49] in 1977 in a Ni-15Cr-6Fe (wt.%) alloy in the temperature range from 673 to 1073 K. The corresponding Arrhenius plot suggested the GB activation energy for Cr diffusion of 179.54 ± 3.60 kJ.mol^{-1} whereas a value of 277.67 ± 4.21 kJ.mol^{-1} was determined for Cr lattice diffusion. Čermák [7] observed the same tendency and demonstrated a strong dependence of the Cr GB diffusivity in polycrystalline Ni-Fe-Cr alloys (with different content in Fe and Cr) on the Cr concentration in the alloys, with a minimum at 10 wt.% Cr [7], which was first investigated by Treheux et al. [50]. A number of similar studies have been conducted in Ni-Cr-Fe alloys [7,51,52], pure Ni and Ni-Cr alloys [7,53–55] but diffusion experiments performed at temperatures lower than 873 K are scarce. Yet, such experiments are imperative to characterize the relaxation of deformation-modified state of GBs.

2. Experimental details

2.1. Material

A Ni material of 2N6 purity (identical to that investigated in Refs. [46,47,56]) was used in the present study. The UFG structure was produced by room-temperature ECAP pressing in the research laboratory of Prof. Y. Estrin (Monash University, Clayton, Australia). Four ECAP (die angle of 90°) passes were employed and the samples rotated by 90° after each pass, as required by the Bc4 process route. No back pressure was applied. The resulting UFG microstructure was investigated in detail in Ref. [57].

2.2. Diffusion study

Diffusion of Cr in UFG Ni was investigated at 403, 503 and 603 K for diffusion annealing of 72 h using both radiotracer measurements and SIMS analysis. The diffusion direction was parallel to the elongation direction of ECAP processing.

Radiotracer measurements

The radioactive isotope ^{51}Cr, in the form of a highly diluted acidic solution, was deposited on polished disc-shaped samples of UFG Ni of 8 mm in diameter and 1 mm thickness. Subsequently, diffusion annealing treatments were carried out in sealed quartz tubes under

purified (5N) Ar atmosphere. After annealing, the diameter of the samples was reduced by approximately 1 mm to remove the contaminant effects of surface and lateral diffusion.

The penetration profiles were determined by the serial sectioning technique using a high-precision grinding machine. Intensity of γ-radiations emitted by radioisotope was counted using intrinsic Ge γ detector. The counting time was chosen to keep the statistical uncertainty of the activity determination below 2%. The background radioactivity was determined by measuring the activity counts from an empty vial. The specific activity which is proportional to the tracer concentration was determined by measuring the mass reduction of the sample after each grinding step. The initial (few) sections (up to 1 μm in total depth) are typically influenced by the calibration procedure of a sample for parallel grinding and/or by very fine surface scales and, therefore, are not included in the analysis of the penetration profiles.

SIMS analysis

A specific experimental procedure detailed in [58] was applied to study Cr diffusion in UFG Ni using SIMS. First, 2-3 mm thick slices of UFG Ni were polished on one face to a mirror-like quality by standard metallographic procedures. A zone of further SIMS analysis was delimited using a AZ50-4 PRESI microhardness tester (the measurements were performed by loading the sample with 4.9 N during a dwell time of 10 seconds). Accordingly, a rectangular zone of 1.5×5 mm² was defined on each specimen. It allowed as well to get the initial hardness of as-produced UFG Ni which was equal to 303 ± 7 HV (averaged on 38 values). The specimens were then coated with a thin Cr film by sublimation of naturally occurring Cr powder (99.95%, Neyco) and condensation onto the polished surfaces in an Emitech K975X thermal evaporator. A targeted Cr thickness of 5 nm was reached by setting an embedded quartz balance with an electrical current equating to 38 A. Subsequently the samples were sealed in quartz tubes under vacuum and diffusion annealing was carried out.

After the diffusion treatment, the SIMS (Cameca IMS 7f) technique was used to measure the intensity profiles as a function of sputtering time. Instead of employing a standard SIMS analysis method, a retrospective approach called “checkerboard analysis” was applied [59]. Each diffusion sample was analyzed together with a corresponding reference sample that has been deposited with natural Cr simultaneously, thus the sputtering-induced profile modifications are thoroughly accounted for. A duoplasmatron $(O_2)^+$ source was employed and the O_2 leak methodology was applied to enhance the positive secondary ion yields [60]. Primary ion energy and current were set to 5 keV and 50 nA, respectively. The isotopes

whose signals were counted during the acquisitions are: ^{50}Cr, ^{52}Cr, ^{54}Cr, ^{58}Ni, ^{60}Ni and ^{64}Ni, together with ^{16}O or ^{56}Fe. In this study, the raster area equates to 150×150 µm² while the analysis area (or region of interest ROI), close to 10×10 µm², was adjusted on the ^{52}Cr ion image, as required when applying the checkerboard analysis method [58].

To determine the sputter rate for each SIMS crater and thereby obtain the diffusion depth profiles from the diffusion profiles over time, the depth of the craters was estimated using a Bruker Dektak 8 contact profiler. A mean sputter rate was calculated for each crater by averaging the crater depth along three horizontal lines crossing the raster area at positions corresponding approximately to 1/4, 1/2 and 3/4 the crater size with an uncertainty of ± 5 µm. The scattering was always below 13% of the mean value. As the intensity profile was extracted from a small part of the crater, a "local" sputter rate was deduced from the local depth values of all the ROIs. The scattering represents approximately 4% of the local sputter rate value averaged over all the craters of the same diffusion experiment [58].

Due to low natural abundance of ^{50}Cr and ^{54}Cr isotopes, the profile for ^{52}Cr was used for further analysis. It is worth noting however that the signals from all Cr isotopes were systematically superposed to check any non-linearity effect between the SIMS counts and concentration [58].

Only the data corresponding to the steady-state acquisition conditions were used for the diffusion coefficient evaluation. The final concentration profile represented the ^{52}Cr/^{64}Ni ratio where the signal from a reference sample (after Cr deposition and without diffusion annealing, the so-called 0-profile) was simply subtracted. More details on the experimental procedure used to get reliable diffusion data in UFG metal using SIMS are available in [58].

2.3 Microstructure characterization

The microstructure of UFG Ni before and after diffusion annealing was characterized using a scanning electron microscope (SEM) S-FEG FEI Nova NanoSEM 450 and electron backscatter diffraction (EBSD) using an acceleration voltage of 15 kV. An area of 20×20 µm² for each sample was scanned with an acquisition step of 30 nm to be able to reveal the features of UFG structure. The as-obtained EBSD maps were analyzed with OIM 7.0 software and with Atex 2.21 software [61]. The former allowed to construct the orientation and image quality (IQ) maps together with GB maps and the latter was used to calculate the density of so-called geometrically necessary dislocations (GND) [62]. Such a multi-parameter EBSD investigation, as it will be discussed further, could reveal the evolution of different

microstructure features on different scales during diffusion annealing. The GND density was obtained using Nye's approach [63] adapted by Panthleon to EBSD analysis [64] as it was done in Ref. [65]. The misorientation of 5° between two neighbor pixels was considered as a threshold to distinguish between the pixels located in different grains. The value of 5° is a typical cut-off value used when "deformation state" is investigated using EBSD. In some recent works (see, for example, [62]), it is shown that the choice of 7, 10 or 15° does not influence the relative results. No filtering of EBSD data was applied before data processing. The initial grain size was measured to be about 300 nm [61].

3. Results

Analysis of diffusion experiments depends on the relevant kinetic regime, classified as A-, B- or C-type after Harrison [66]. In the C-kinetic regime, which is followed typically at lower temperatures and shorter annealing times, the tracer diffusion into the bulk is negligible and atomic transport occurs primarily along the grain boundaries and, thus, the true GB diffusion coefficient can be determined. In order to demarcate B- and C-type kinetic regimes, the value of the Le Claire parameter α is decisive [67] (Eq. (1))

$$\alpha = \frac{s\delta}{2\sqrt{D_v t}}. \quad (1)$$

Here, s is the segregation factor and δ is the diffusional GB width (measured to be equal to about 0.5 nm in 85 FCC metals [56]), D_v is the bulk diffusion coefficient and t is the annealing time. D_v was calculated using the parameters determined in [7] (Eq. (2)):

$$D_v = 8.61 \times 10^{-4} \times exp\left(\frac{-288.6\ kJ\ mol^{-1}}{RT}\right), \text{m}^2\ \text{s}^{-1}. \quad (2)$$

A reliable α estimation requires the segregation factor to be known. In the present conditions, we found that $\alpha >> 1$ even in the case of $s = 1$ (Table 1). Thus, the C-type kinetic regime conditions are safely satisfied [68] for all the measurements. Note that the absence of Cr segregation to Ni Σ11 grain boundaries was confirmed by theoretical calculations using the density function theory [69,70].

Table 1: Experimental parameters for Cr diffusion experiments in UFG Ni, $\sqrt{D_v t}$ and α are calculated according to the data from Eq. (2) [7] and using Eq. (1), respectively.

Temperature (K)	Time (s)	$\sqrt{D_v t}$ (nm)	α
403	259200	3.0×10^{-9}	8.5×10^{9}
503	259200	1.5×10^{-5}	1.6×10^{6}
603	259200	4.7×10^{-3}	5.3×10^{3}

3.1. Radiotracer measurements

In the case of radiotracer experiments, the Gaussian (thin film) solution can typically be applied and the logarithm of the tracer concentration, $\bar{c}$, is found to be proportional to the penetration depth squared, x^2. Thus, the grain boundary diffusion coefficient, D_{gb}, can be directly determined using Eq. (3)

$$D_{gb} = -\frac{1}{4t}\left(\frac{\partial ln\bar{c}}{\partial x^2}\right)^{-1}. \quad (3)$$

Figure 1 shows the penetration profiles measured at 403, 503 and 603 K by the radiotracer technique. After an initial drop of the tracer activity by more than two orders of magnitude (which corresponds to the given density of the short-circuit paths in the sample and is affected by the grinding-in effects), a prolonged tail corresponding to GB diffusion is observed. An increase by a factor of twenty is found for the GB diffusion coefficient when the temperature increases from 403 to 603 K (Table 2).

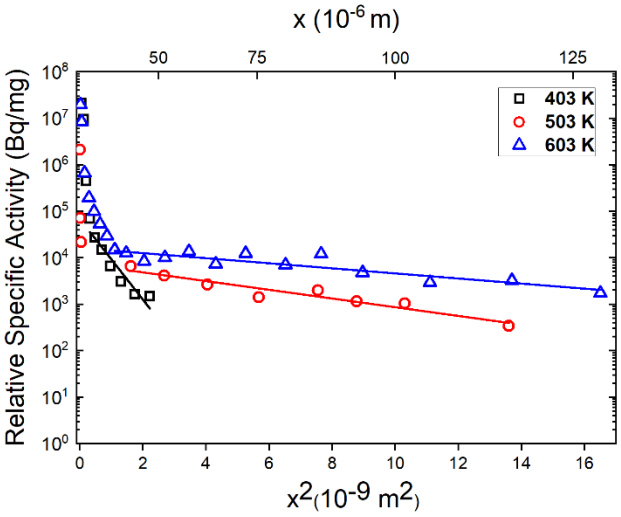

Figure 1: Penetration profiles of ^{51}Cr GB diffusion in UFG Ni during 72 h at 403, 503 and 603 K obtained by radiotracer technique.

3.2. SIMS measurements

Considering a 5 nm-thick Cr layer deposited on the UFG Ni surface for SIMS measurements and a negligible bulk diffusion distance (which is far below 1 Å, Table 1), a constant source solution was applied for analyzing the concentration profiles obtained by SIMS (Eq. (4)),

$$\bar{c}(x,t) = c_s + (c_0 - c_s) \times erf\left(\frac{x-x_0}{2\sqrt{D_{gb}t}}\right), \quad (4)$$

where c_s is the tracer concentration at reference x_0 coordinate and c_0 is the background level (obtained at very large depths).

As mentioned in the Experimental part section, SIMS concentration profiles can be obtained by using the local or mean sputter rate. Nevertheless, the corresponding values of the diffusion coefficients were found to be similar, within the experimental uncertainty. Therefore, for the sake of concision and clarity, here, only the results considering the local sputter rate are presented.

Table 2: Cr GB diffusion coefficients in UFG Ni obtained by SIMS and radiotracer technique at different temperatures and annealing of 72 h. The SIMS profiles are referenced, according to Figure 2.

Temperature (K)	Diffusion coefficient ($\times 10^{-21}$ m² s^{-1})		
	SIMS		Radiotracer
	Profile	Value	
403	1	0.2 ± 0.9	3800^{+1700}_{-600}
	2	0.3 ± 4	
	3	3.7 ± 0.5	
	4	0.9 ± 17	
	5	0.1 ± 0.3	
503	1	0.31 ± 0.2	44800^{+14000}_{-1200}
	2	0.36 ± 0.2	
603	1	0.73 ± 0.08*	76500^{+6000}_{-6500}
	2	0.29 ± 0.4*	
	3	2.5 ± 0.2*	

*GB diffusion coefficients obtained at 603 K have no physical meaning due to microstructure evolution during the diffusion experiment (see below).

Figure 2 presents the obtained penetration profiles together with the corresponding fitting functions, according to Eq. (3), for all the analyzed craters. The determined diffusion coefficients are reported in Table 2. One can see that for the same annealing conditions, the diffusion coefficients are scattered over an order of magnitude. All values are within 10^{-22} – 10^{-21} m^2s^{-1} range, and they differ by a factor of 10^3 – 10^5 from the diffusion coefficients obtained by the radiotracer technique. Such a scatter of the SIMS data for the same diffusion annealing conditions is explained by the local character of the SIMS analysis (the signal is averaged over areas of tens of μm^2) while the radiotracer technique analyses the signal averaged over the area of tens of mm^2.

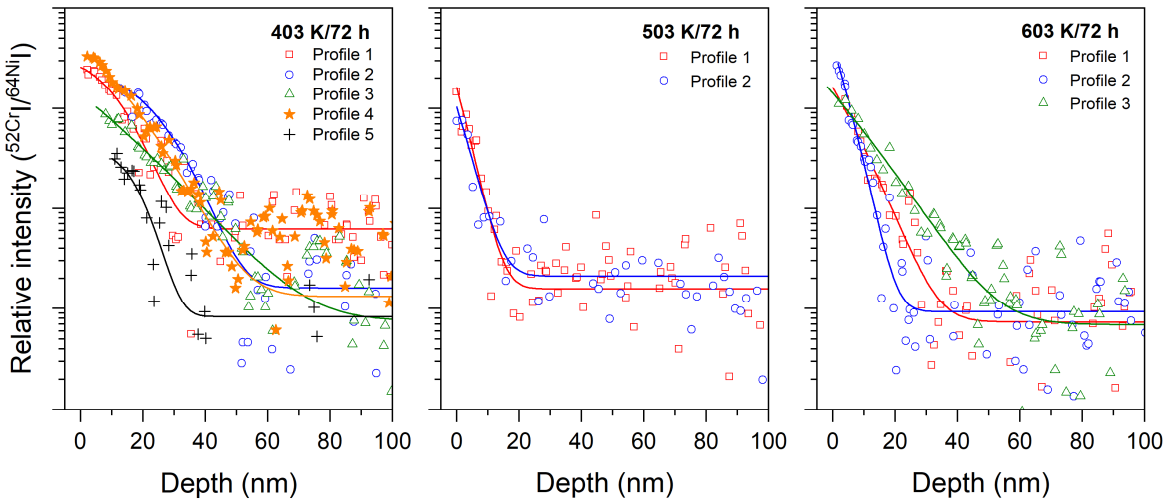

Figure 2: Penetration profiles of Cr diffusion in UFG Ni obtained by SIMS after diffusion annealing for 72 h at (a) 403 K, (b) 503 K and (c) 603 K.

3.3. UFG microstructure

As previously reported by Divinski et al. [71], the same UFG Ni exhibits a nearly constant microhardness values up to the temperatures of 600 K when it is annealed for 17 h. In the present study (annealing time 72 h), the measured microhardness after diffusion treatment at 403 K was equal to 322 ± 16 HV, slightly above the initial value (303 ± 7 HV). This slight increase in microhardness after annealing at 400–500 K was also observed in [71] and in high-pressure torsion deformed Ni specimens [72] and attributed to depletion of dislocation sources after vacancy annihilation and additional dislocation pinning by vacancy clusters. However, a complete survey of this topic is beyond the scope of the present paper. After 503 and 603 K diffusion treatments, the measured microhardness values slightly decreased to 288 ± 6 and 289 ± 28 HV respectively, suggesting a certain microstructure evolution.

According to the DSC analysis of as-received UFG Ni (without diffusion annealing) [71], dislocation recovery is expected from about 500 K and a noticeable grain growth occurs above 600 K. It can be thus supposed that no significant microstructure evolution occurred during diffusion annealing at 403 and 503 K while it could take place at 603 K. However, it is worth noting that the DSC experiment was carried out at a constant heating rate of 20 K.min^{-1} and the transformation temperatures obtained in Ref. [71] are overestimated when compared to isothermal conditions. Thus, some microstructure evolution at 503 K during annealing for 72 h can be expected.

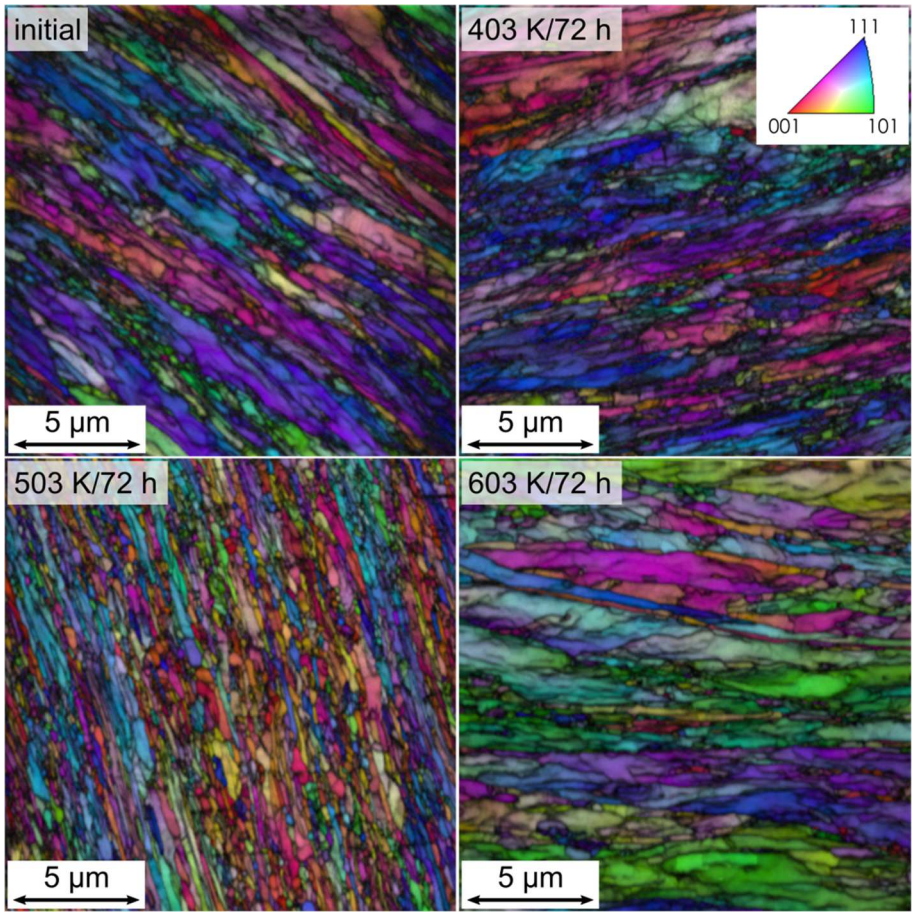

Figure 3: Orientation maps coded in normal direction to sample surface (which is parallel to the elongation direction of ECAP processing and diffusion direction) superposed with IQ maps for the samples of UFG Ni used to study Cr diffusion: initial state (without diffusion annealing) and after diffusion annealing at 403, 503 and 603 K for 72 h (acquisition step is 30 nm). (For interpretation of the references to color in this figure legend, the reader is referred to the web version of this article).

The microstructure evolution, i.e. before and after diffusion annealing treatments, was investigated using SEM/EBSD. The orientation maps coded in normal direction to sample surface superposed with IQ maps are shown in Figure 3. An UFG structure is clearly observed for all samples. No visible microstructure modification is detected after annealing at 403 K. After annealing at 503 K, ultrafine grains are still observed but they look more well-defined, suggesting that some microstructural changes might occur. At last, the sample annealed at 603 K during 72 hours has obviously coarser grains in comparison with other samples suggesting thus a non-negligible grain structure evolution and grain growth during the diffusion annealing.

Furthermore, IQ maps were superposed to GB maps (Figure 4) and the GB length per GB character (normalized by the analyzed surface) was calculated and reported in Table 3. No significant change of the GB length is found between the initial state and that after diffusion

annealing at 403 K, as close densities of low- and high-angle GBs are obtained. The annealing treatment at 503 K keeps as well the same quantity of low-angle GBs, as compared to the initial state and that after annealing at 403 K, while a slight decrease of the fraction of high-angle GBs can be suggested. Annealing at 603 K for 72 h is found to result in a remarkably different grain structure as compared to other samples. A three- to four-fold decrease of the density of high-angle GBs is clearly seen (Table 3).

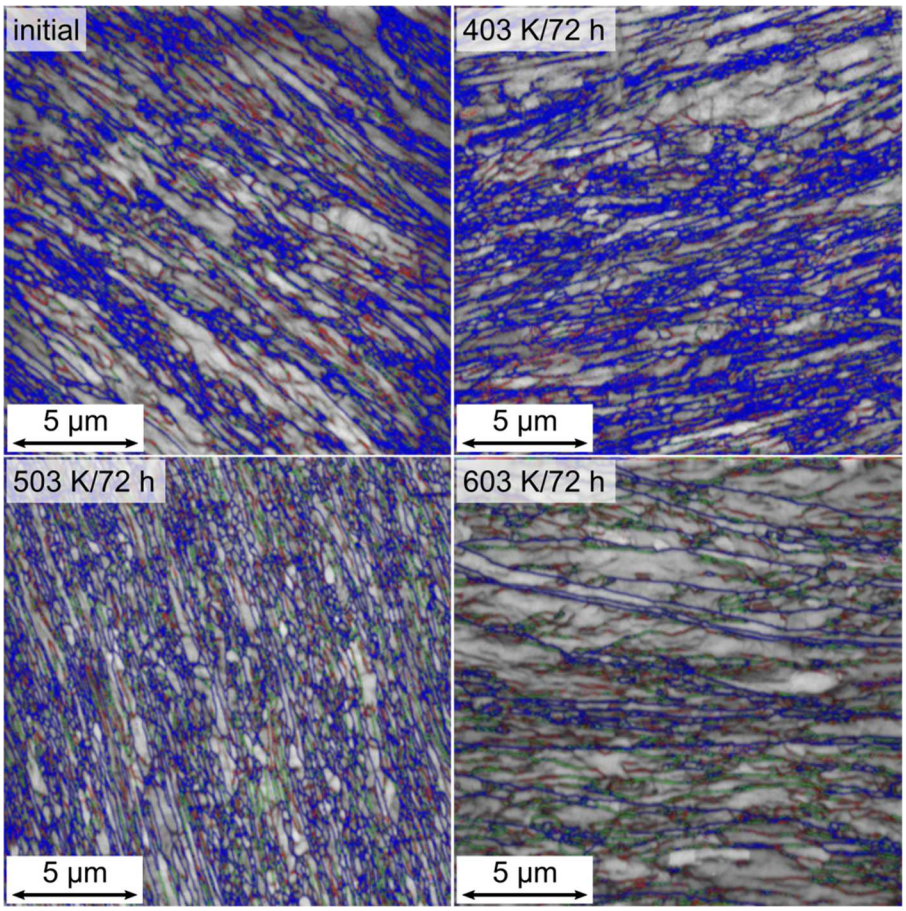

Figure 4: IQ maps superposed with GB maps, as obtained by EBSD for the samples of UFG Ni used to study Cr diffusion: initial state (without diffusion annealing) and after diffusion annealing at 403, 503 and 603 K for 72 h (acquisition step is 30 nm). GB with misorientation angle higher than 15° are in blue; those with misorientation angle within 5 and 15° are in green and those with misorientation angle within 2 and 5° are in red. (For interpretation of the references to color in this figure legend, the reader is referred to the web version of this article).

Table 3: GB length surface density per GB character and mean GND density obtained from EBSD analysis on UFG Ni before and after diffusion annealing.

Conditions of diffusion annealing	Mean of sub- and GB length surface density for different GB misorientation angles (μm μm^{-2})	Mean GND density (m^{-2})
Initial state (without diffusion annealing)	2.9 (2-5°) 1.2 (5-15°) 13.5 (>15°)	3.3×10^{15}
403 K/72 h	2.4 (2-5°) 1.1 (5-15°) 16.6 (>15°)	3.3×10^{15}
503 K/72 h	2.3 (2-5°) 1.8 (5-15°) 10.1 (>15°)	2.8×10^{15}
603 K/72 h	1.5 (2-5°) 1.3 (5-15°) 3.1 (>15°)	2.1×10^{15}

To get a further insight into possible microstructure evolution during the diffusion annealing, the GND density was calculated for all the samples. The GND density distribution can be reliably represented by Rayleigh [73,74] or lognormal [62] distributions. In the present work, the lognormal distribution was found to be more appropriate to describe the experimental results (Figure 5). Therefore, the GND density obtained from EBSD was fitted using Eq. (5):

$$f(\rho_G|\mu,\sigma) = \frac{1}{\rho_G\sigma\sqrt{2\pi}} exp\left(-\frac{(ln(\rho_G)-\mu)^2}{2\sigma^2}\right), \quad (5)$$

where ρ_G is the GND density and μ and σ are fit parameters. Accordingly, the mean GND density is defined, according to Eq. (6) (Table 3)

$$\overline{\rho_G} = exp\left(\mu + \frac{\sigma^2}{2}\right). \quad (6)$$

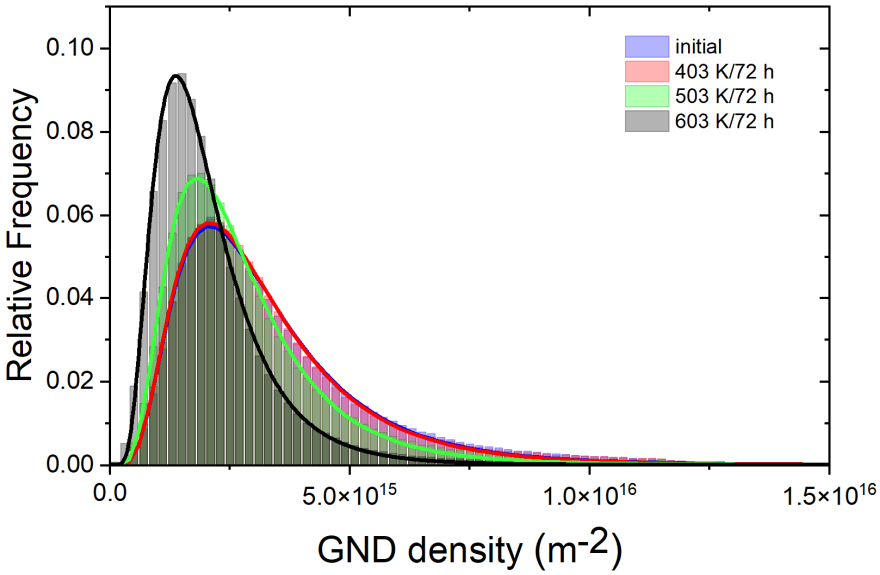

Figure 5: GND density distribution obtained using EBSD data and Nye's approach [63] adapted by Pantleon [64,65] for EBSD data in UFG Ni in initial (as processed by ECAP) state (in blue) and after diffusion annealing for 72 h at 403 (in red), 503 (in green) and 603 K (in black). The distributions were fitted using log-normal function (Eq. (5)) to get mean values (Eq. (6)) reported in Table 3. The blue and red curved are almost indistinguishable. (For interpretation of the references to color in this figure legend, the reader is referred to the web version of this article).

The GND density distributions are identical for UFG Ni in the as-received state and after annealing at 403 K for 72 h (blue and red curves, respectively in Figure 5). A slight difference is induced by annealing at 503 K (green curve in Figure 5). The mean GND density is slightly lower and the distribution slightly narrower compared to the two previous samples, suggesting that a rearrangement of the dislocations has already begun. Nevertheless, the difference is within the experimental uncertainty of the method. On the contrary, after annealing at 603 K, a significant decrease of the mean GND density is observed (Table 3). The distribution is also significantly narrower and shifted towards the lower values (black curve in Figure 5) confirming previous conclusions on recovery process at such diffusion conditions. Therefore, the characterization of the UFG Ni samples before and after diffusion annealing has undoubtedly shown a microstructure evolution after annealing at 603 K for 72h.

According to the Evans and Glaeser model [75], GB migration during a diffusion experiment modifies significantly the tracer distribution resulting in a linear decay of the logarithm of the tracer concentration with depth and the corresponding slope is given by Eq. (7)

$$\frac{\partial ln\bar{c}}{dx} = -\sqrt{\frac{V_m}{\delta D_{gb}}}. \quad (7)$$

Here V_m is the mean GB velocity. Therefore, using the slopes of Cr concentration profiles in UFG Ni obtained by SIMS (Figure 2) and that one characterizing the first near-surface branch of the radiotracer penetration profile measured at 603 K (Figure 1), the mean GB velocities and thus the mean GB displacements during diffusion annealing can be estimated. As one can see from Eq. (7), such estimation requires the GB diffusion coefficient to be known.

It is still a matter of debate whether the solute diffusion coefficient for stationary and mobile GBs is the same or not [76,77]. Up to five orders of magnitude of enhancement of the GB diffusion rate via mobile boundaries was reported in minerals [78], while detailed investigations of discontinuous precipitation reactions in metallic alloys collaborated a view that the solute diffusion coefficients are similar for stationary and mobile GBs [79,80]. Furthermore, systematically similar values for GB migration were elaborated in tracer diffusion experiments using different solutes in the same Cu matrix [81] that supports the previous findings [82] if the diffusion-induced grain boundary migration (DIGM) phenomena could safely be excluded.

If we would interpret the penetration profiles measured by SIMS (Figure 2) and the first (near-surface) branch of the radiotracer diffusion profile measured at 603 K (Figure 1), as the consequence of Cr diffusion along migrating GBs, we may estimate the migration rates V_m using the appropriate GB diffusion coefficients. In the present work, the Cr GB diffusion coefficients in UFG Ni as measured by the radiotracer technique are reported in Table 2. On the other hand, Cr GB diffusion in a coarse-grained 3N6 Ni was previously reported by Čermák et al. [7]. It is instructive to use both sets of data for Cr diffusion in Ni to estimate the mean GB displacements during the diffusion annealing treatments using Eq. (7) and the results are shown in Figure 6.

On one hand, if we would tentatively use the Cr GB diffusion rates measured by the radiotracer technique, the mean GB displacements appear to be larger than 10 µm and can even reach 1 mm for 503 and 603 K. Such pronounced grain growth has to be easily detected by EBSD, which is in obvious contradiction with the observed microstructure evolution in Figure 3 and Figure 4. Therefore, it is not the GB displacement with the rates measured by the radiotracer technique which would correspond to the SIMS profiles. In other words, the SIMS profiles do not correspond to the motion of the GBs which provide simultaneously the deep penetration of the solutes detected by the radiotracer technique.

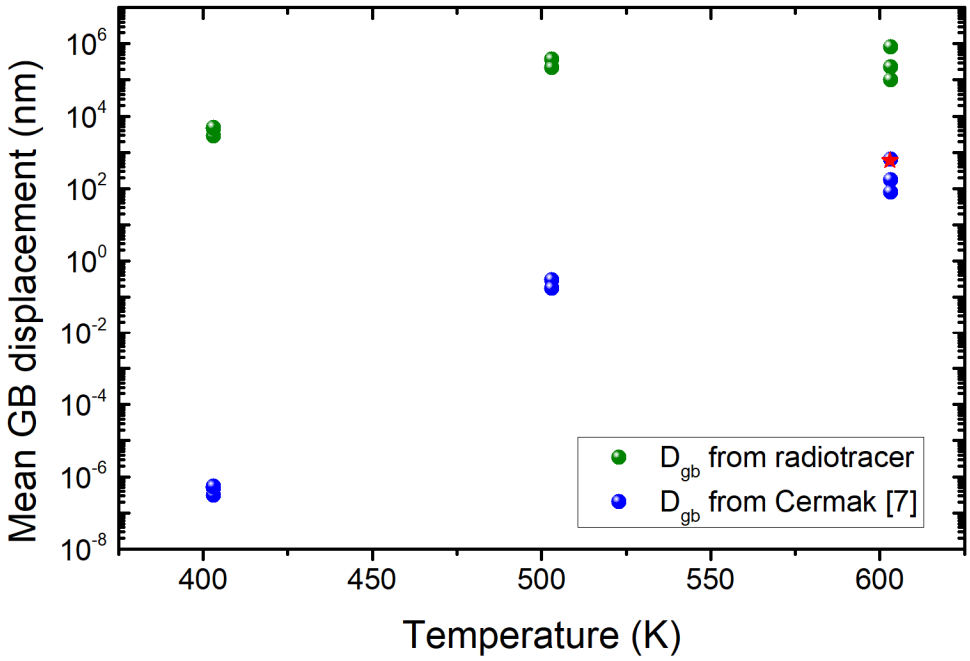

Figure 6: Mean GB displacement during diffusion annealing for 72 h at different temperatures, as estimated using the Evans and Glaeser model (Eq. (7)) and taking Cr GB diffusion coefficients in Ni as obtained by Čermák in coarse-grained Ni [7] (blue spheres) and in the present work by the radiotracer technique in UFG Ni (green spheres). Grain boundary displacement evaluated from the microstructure analysis at 603 K are indicated by red star. At lower temperatures, no grain growth was detected. (For interpretation of the references to color in this figure legend, the reader is referred to the web version of this article).

If one would interpret the SIMS profiles as resulting from the motion of GBs, which GB diffusion coefficients correspond to Čermák's data for coarse-grained Ni, one arrives at a more consistent picture. Indeed, no GB migration should occur at 403 K, a negligible GB displacement of about 1 nm is predicted at 503 K and a significant (for the UFG structure) GB displacement of about 1 µm should occur at 603 K. The latter estimate is in a perfect agreement with the basically independent microstructure analysis according to the SEM/EBSD data (Figure 3 and Figure 4).

Taking into account the results presented above, we are forced to conclude that the diffusion experiments were carried out in almost stable UFG structure of Ni at 403 and 503 K while the microstructure underwent significant evolution during the diffusion annealing at 603 K. Therefore, both SIMS and radiotracer data obtained for 403 and 503 K reveal the real GB properties of UFG Ni at these temperatures, although the corresponding diffusion rates differ by orders of magnitude. On the other hand, the diffusion coefficients measured by the radiotracer technique at 603 K are reasonable, while the SIMS profiles at this temperature

correspond to the tracer distribution built up by moving GBs. Moreover, the GB diffusion coefficients for the moving boundaries correspond to the diffusion rates observed in well-annealed coarse-grain polycrystals.

4. Discussion

In the present work, GB diffusion of Cr in UFG Ni was investigated by both SIMS analysis and the radiotracer technique and an important difference in the determined values, by three to five orders of magnitude, was observed (Table 2). Moreover, almost similar GB diffusion coefficients at 403 and 503 K were measured by SIMS (see the Arrhenius diagram in Figure 7). These features have to be clarified and the specific GBs addressed by different methods at different temperatures have to be identified.

4.1 Correlative cross-scale study by SIMS and radiotracer analyses

To discuss the difference in the Cr GB diffusion coefficients for a given temperature, one has to consider that SIMS and radiotracer technique provide access to the concentration profiles from *fundamentally* different penetration depths due to the different detection limit. As one can see in Figure 1 and Figure 2, the concentration profiles obtained by the radiotracer technique could be processed for the depths up to 100 µm while those acquired by SIMS gave the data above background level for the depths less than 50 nm. As it was stated in the Introduction, a co-existence of GBs with different metastability states, relaxed and non-relaxed GBs, was reported in UFG Cu or Ni [42,43]. The corresponding two branches of concentration profiles were called as fast and ultra-fast short-circuits, having in mind that the relatively slower ("fast") branch provides GB diffusion rates corresponding to general high-angle GBs as they are observed in annealed polycrystalline (coarse-grained) materials [42]. While both such contributions were possible to measure simultaneously for UFG copper using the radiotracer technique [42], only indirect hints to the existing hierarchy in UFG Ni were stated [32]. The reason is the difference of the corresponding diffusivities, while it occurred to be about an order of magnitude in UFG Cu [42], it has to be more than two orders in UFG Ni [32]. Are the "fast" diffusion coefficients in UFG Ni of the same level as in polycrystalline Ni or somewhat enhanced, this fundamental question remained unresolved.

The present combination of basically two different diffusion techniques allows unprecedented insights into the hierarchy of short-circuit paths in UFG Ni allowing cross-scale characterization of the pertinent diffusion coefficients.

The relaxed GBs are considered to possess the same properties as the GBs in a standard coarse-grained metal. On the other hand, non-relaxed and thus high-energetic GBs have significantly different properties and they might evolve to a relaxed state during, for instance, recovery induced by temperature exposure of UFG metal. In other words, non-relaxed GBs have significantly increased GB diffusion coefficient as compared to relaxed GBs [42,83]. As it was suggested in previous studies [42,43], the fraction of non-relaxed GBs in UFG Ni should not exceed 10% and their contribution to mass transport is therefore "hidden" by slower, relaxed GBs. However, the situation can be different when the mass transport is studied at depths where the contribution from relaxed (and slow) GBs is negligible while that from non-relaxed (and fast) GBs is still significant (Figure 8). This is exactly what happens when GB diffusion is studied by both SIMS and radiotracer technique: the latter gives the properties of non-relaxed and "ultra-fast" GBs (at large penetration depths) while the former gives the properties of relaxed and "fast" GBs (at short penetration depths). Therefore, the difference in GB diffusion coefficients by three to five orders of magnitude as obtained by SIMS and radiotracer methods (Table 2) reveals the co-existence of GBs with different metastability levels in UFG Ni produced by ECAP. In spite of a low density of the ultra-fast paths, their contribution could reliably be resolved in deep sections by the radiotracer technique due to integration of the signal over the whole sample section. On the other hand, the SIMS analysis is basically local and representative for the small depths where the majority of relaxed paths dominate the solute distribution (Figure 8). Hence, the results from SIMS have to be compared with the data on Cr GB diffusion in coarse-grained Ni available in the literature (Figure 7).

The green (radiotracer) and red (SIMS) symbols in Figure 7 represent the measured contributions of "ultra-fast" (deformation-modified [43]) and conventionally "fast" (relaxed) high-angle GBs. The Cr diffusion rates in deformation-modified GBs (green circles) are found to be somewhat lower than those of matrix Ni atoms (black dotted line), Figure 7, but the two data sets follow similar trends. The Cr GB diffusion coefficients in 2N6 UFG Ni are extremely higher than those predicted from measurements by Čermák in 3N6 coarse-grained Ni [7] when these are extrapolated to low temperatures (solid blue line, Figure 7). This fact substantiates the deformation-modified state of high-angle GBs in UFG Ni produced by ECAP processing.

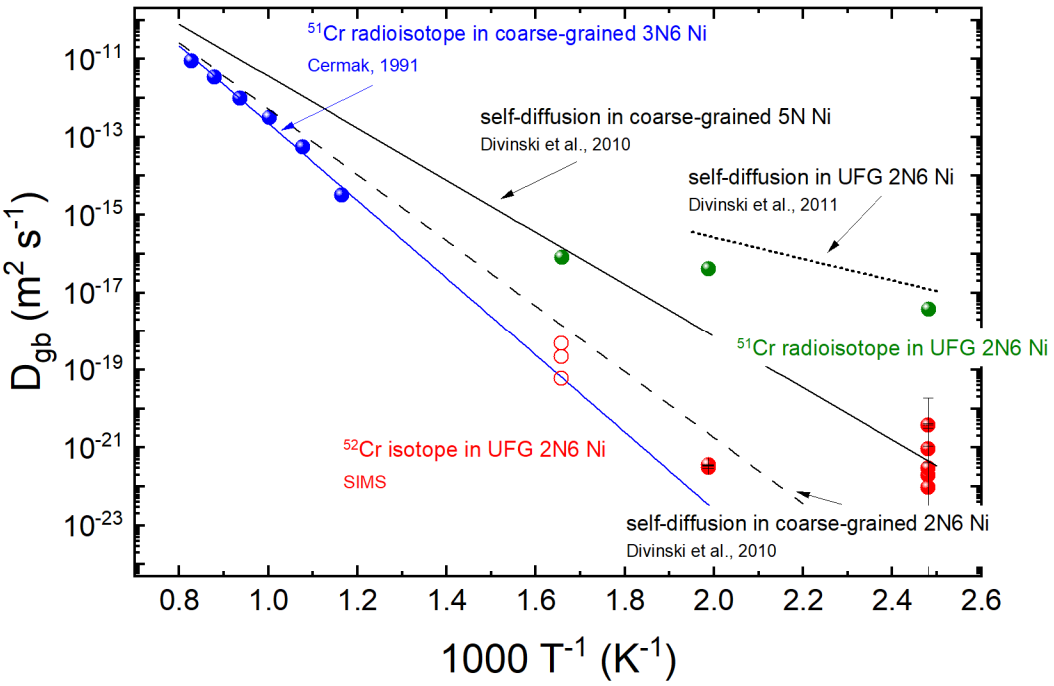

Figure 7: Temperature dependence of measured GB diffusion coefficients of Cr in UFG 2N6 Ni as obtained by SIMS (in red) and by radiotracer technique (in green), as compared to that measured by Čermák in coarse-grained 3N6 Ni (in blue) [7]. GB Ni self-diffusion coefficients in coarse-grained 2N6 and 5N Ni [84] and in UFG Ni [32] are shown as well. For the SIMS data, the GB diffusion coefficients at 603 K (open red circles) were estimated accounting for the grain structure evolution and using Eq. (6), see text. (For interpretation of the references to color in this figure legend, the reader is referred to the web version of this article).

For the first time, a second contribution to Cr transport in UFG Ni is measured by SIMS analysis (red symbols, Figure 7). The corresponding diffusion coefficients are by three to five orders of magnitude lower than those for deformation-modified GBs. Simultaneously, these values exceed significantly, by many orders of magnitude those predicted for relaxed high-angle GBs as they are present in coarse-grained 3N6 pure Ni after Čermák [7] at 403 K, whereas quite similar values for the two data sets are found at 503 K.

Interestingly, Cr GB diffusion in 2N6 UFG Ni at 403 K occurs with similar rates being characteristic for Ni self-diffusion in coarse-grained high-purity 5N Ni (Figure 7). Although Cr heterodiffusion in Ni cannot be unambiguously compared with Ni self-diffusion, it can be speculated that the increased Cr GB diffusivity in as-processed UFG 2N6 Ni (with a high density of GBs), as compared to that in coarse-grained 3N6 Ni (with a lower density of GBs), can be explained by the "GB purification" effect as suggested by Prokoshkina et al. [56]. Impurities present in the 2N6 UFG Ni before ECAP were redistributed over a significantly larger number of newly formed GBs after ECAP processing, including dislocations and low-

angle GBs, leading to a higher purity of GBs, comparable to the one of the 5N coarse-grained Ni. This finding is in line with the well-known impact of the material purity of both self- [56,84,85] and solute [86] diffusion. The GB diffusion rates as measured by SIMS at 403 K reveal a large intrinsic heterogeneity of the kinetic properties of individual boundaries. This dispersion indicates an absence of appreciable relaxation of the high-angle GBs and correlates with the existence of broad-spectrum boundaries with significantly different properties.

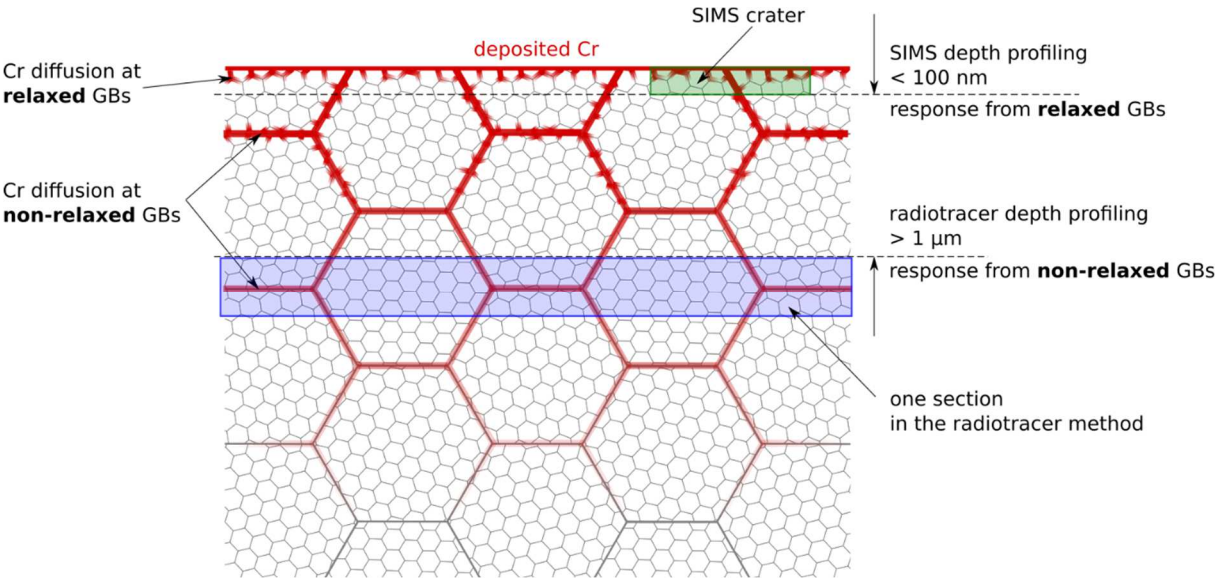

Figure 8: A scheme of contribution of relaxed and non-relaxed GBs in UFG Ni to Cr diffusion at different depths as studied by SIMS and radiotracer technique at the conditions of the C-regime.

At 503 K, Cr GB diffusion coefficient in 2N6 UFG Ni as measured by SIMS approaches that in coarse-grained 3N6 Ni (and is close to Ni self-diffusion coefficient in the *same* 2N6 coarse-grained Ni) (Figure 7). As it was stated previously, at 503 K, some minor microstructure changes occurred triggered by annihilation of deformation-induced vacancies, formation and motion of vacancy-impurity pairs and dislocation recovery [87]. These processes contribute to interface relaxation, leading to lower Cr GB diffusion coefficients measured at 503 K. Moreover, due to these "minor" microstructure changes, mainly due to vacancy drag effect, solutes can be redistributed over different GBs, thereby erasing the abovementioned purification effect, and leading to GB properties in 2N6 UFG Ni (even slower) comparable with those in 3N6 coarse-grained Ni (Figure 7).

At 603 K, the measured SIMS profiles are governed by tracer diffusion along migrating boundaries. Estimating the averaged boundary migration rate from the measured grain growth

after annealing for 72 h and using Eq. (6), the Cr GB diffusion coefficients can be evaluated and the results are given in Figure 7 (open red circles). These values are in a nice agreement with the Cr diffusion rates in coarse-grained relaxed Ni.

It is worth noting that this particular study does not focus on specific GB states. Detailed high-resolution TEM investigation is required for that, which however is very difficult to correlate with diffusion measurements. Inherently, TEM investigation is highly local (GB fraction of several hundreds of nanometers in length is examined), which diffusion property is averaged over GBs of 20 to 100 μm^2 (in the case of SIMS) or ≥ 10 mm^2 (using the radiotracer method). In the case of UFG Ni (with the grain size of about 300 nm), we cannot quantify the diffusion properties of a single GB, that would be possible for bicrystals, for example. In the present work, we have observed a relaxation of GB diffusion rates without a strong modification of microstructure (with respect to GB misorientations/inclinations) in pure Ni. This is why we believe that fastest paths are non-equilibrium GBs which relax.

It should be emphasized that one should distinguish between non-relaxed GBs and sub-grain boundaries. By ECAP processing, we produce a material with a multi-level hierarchy of short circuits with respect to their diffusivities (exceeding those of the crystalline bulk). In the case of non-segregating solutes, these are (classified by increasing diffusion coefficients):

(i) coherent twin boundaries;

(ii) single dislocations, dislocation walls and low-angle GBs;

(iii) incoherent twin boundaries;

(iv) high-angle GBs;

(v) non-relaxed high-angle GBs;

(vi) porosity.

Segregation might somehow bias the classification. This classification seems to be valid for pure Cu and Ni. At a given temperature, the scatter of the pertinent diffusivities for the paths (i) and (ii) is relatively small. Relatively large scatter is expected for (iii), depending on particular inclination of twin boundary. In the case (iv), the variation of grain boundary diffusion coefficient is significant, depending on a lot of GB parameters (inclination, misorientation, GB “phase”, etc.). Using the spectrum of computed GB energies and the

Borisov's approach [92] (see below for further details), one may estimate the range of possible diffusion coefficients for high-angle GBs in a material. The values measured for (v) are by orders of magnitude larger.

If we have a coarse-grained Ni with developed sub-grain structure (produced via rolling), no diffusion would be measured under the conditions of the present paper [90]. Thus, we do know that this is not a combination of (ii) and (iv) which can explain our results.

4.2. GB energy as determined by diffusion measurements

Together with GB diffusion coefficient, GB energy is another GB property of crucial importance which can inform on GB state. In the case of self-diffusion in pure metals, GB energy γ_{gb} can be estimated using the self-diffusion coefficients in the bulk (D_v) and in the GB (D_{gb}) via semi-empirical Borisov's equation [88,89] (Eq. (8))

$$\gamma = \frac{RT}{2\Delta_m^2 N_A} \ln \frac{D_{gb}}{D_v}, \tag{8}$$

where N_A is the Avogadro's constant, R the gas constant and Δ_m means the distance between atoms at the GB. The validity of Borisov's equation for the self-diffusion in binary alloys was discussed in Refs. [56,91,92]. It was suggested that Borisov's equation can be confidently used for the systems where the alloying element does not segregate at GBs (or the segregation is low) and some development was proposed for the systems with strong segregation solutes.

Recently, the Borisov formalism was extended to the case of solute diffusion, both substitutional [93] as well as interstitial [94]. We argue that this analysis can be applied to estimate GB energy using the substitutional solute GB diffusion coefficient if the following two conditions are fulfilled: (i) the solute does not segregate at GBs and (ii) the solute GB diffusion coefficient is close to that of the solvent. Cr is not expected to segregate at Ni GBs due to high solubility limit from 20 to 30 at. % in the temperature range from 403 to 603 K [95–97]. Moreover, as one can see from Figure 7, Cr has almost identical GB diffusion coefficient in 3N6 as compared to Ni self-diffusion coefficient in 2N6 Ni, especially, when high temperature values are compared. Some difference is observed at low temperatures which might be due to extrapolation accuracy. Therefore, we believe that Cr GB (and bulk) diffusion coefficient in Ni can be used to estimate Ni GB energy applying Borisov's equation (Eq. (2)). For the mean distance between atoms at the GB, Δ_m, the Ni lattice parameter at room temperature was used but it had no significant effect on the calculation

results presented in Figure 9. The Cr bulk diffusion coefficient was taken according to Růžičková et al. (Eq. (9)) [55,98],

$$D_v = 1.6 \times 10^{-3} \exp\left(-\frac{300\ \text{kJ mol}^{-1}}{RT}\right),\ \text{m}^2\ \text{s}^{-1} \tag{10}$$

First, one can see that the GB energies predicted using the radiotracer data are higher than those obtained using the SIMS results, since different GB states were accessible for the experimental study by these techniques (relaxed GBs for SIMS and non-relaxed, deformation-modified GBs for the radiotracer technique).

Figure 9 substantiates that the same interfaces, i.e. the deformation-modified GBs, were measured by the radiotracer analysis of Cr (the present work) and Ni [32] diffusion. The agreement is amazing, since basically different data sets with respect to self- and solute diffusion in crystalline bulk and along grain boundaries were used for the estimates. Such a result confirms that the GB energies can indeed be reliably estimated from the heterodiffusion data if the solute has close diffusion properties to the solvent and does not segregate to solvent GBs.

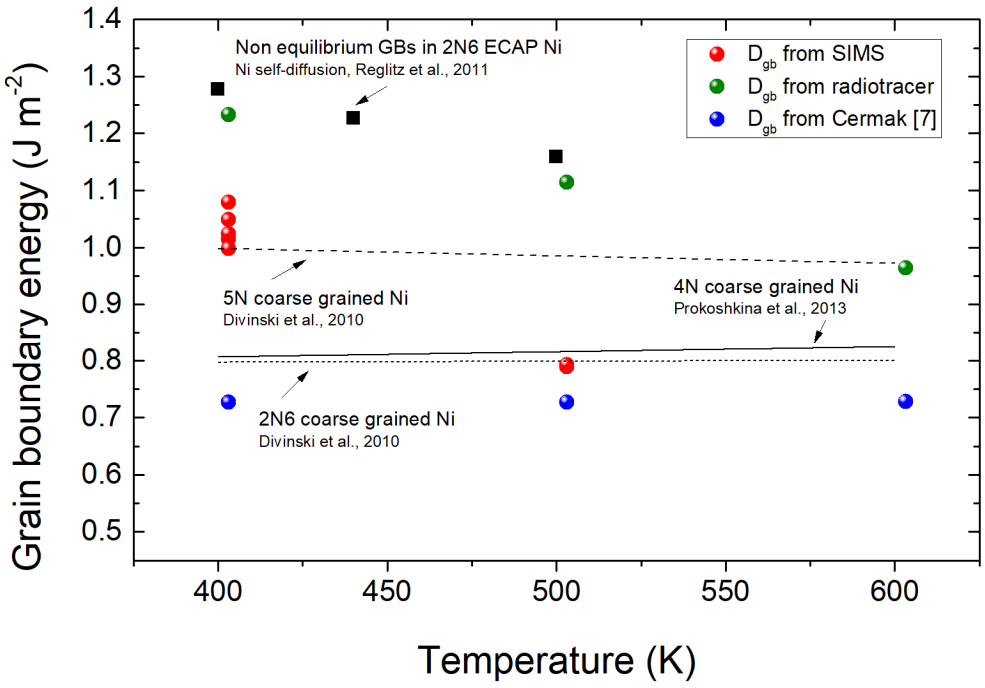

Figure 9: GB energy in UFG 2N6 Ni estimated using Borisov's equation (Eq. (2)) and Cr GB diffusion obtained by SIMS and radiotracer technique (data from the present work) as well as that obtained by Čermák in coarse-grained 3N6 Ni. The Cr bulk diffusion coefficient was taken, according to Růžičková et al. [55,98]. GB energy in the *same* UFG and coarse-grained 2N6 Ni as well as that in 5N coarse-grained Ni obtained from self-diffusion measurements are given for the comparison.

The determined GB energies of relaxed interfaces support completely our interpretation of the SIMS data. At 403 K, the GB energies obtained using the SIMS data are higher than that estimated using Čermák's data in coarse-grained 3N6 Ni and are in agreement with the results for highly pure Ni, black dashed line (Figure 9) suggesting GB purification in UFG metal, as discussed above. Moreover, the spectrum of GB energies determined by SIMS analysis at 403 K, spread over 0.1 J m^{-2}, corresponds to that predicted by atomistic calculations for relaxed high-angle GBs with different misorientation parameters [99].

At 503 K, the GB energies obtained using the SIMS data in UFG 2N6 Ni and that using Čermák's data in coarse-grained 3N6 Ni have similar values in agreement with previous discussion on GB relaxation in UFG Ni. Then, due to GB relaxation, energy of relaxed GBs approaches that of GBs in the *same* Ni with coarse grains.

Therefore, a combined SIMS–radiotracer investigation of Cr GB diffusion in UFG 2N6 revealed the co-existence of GBs with different diffusion properties. A diffusion study revealed once again [100] to be a very powerful, and perhaps unique, tool not only to get the data on mass transport, but also to probe existence and thus the properties of different multi-level hierarchic microstructure features.

5. Conclusions

Cr diffusion in ultrafine-grained 2N6 Ni is measured using two complementary techniques, the radiotracer method and SIMS analysis (in parallel sectioning mode). These two methods are naturally characterized by fundamentally different accessible depths as well as depth and lateral resolutions. While the radiotracer technique and the SIMS analysis, being complementary with respect to the addressable temperature/time windows, yield the same information with respect to bulk diffusion in crystalline materials, basically different grain boundaries/grain boundary states/grain boundary facets are shown to be accessible by these techniques in polycrystalline materials of a complex, multi-level hierarchic microstructure.

Whereas the radiotracer technique in combination with the parallel sectioning method yields the layer concentrations of diffusing atoms integrated over the whole sample section, the SIMS analysis in the so-called checker-board mode is powerful to provide local depth profiles being characteristic for areas of about 10×10 μm^2.

The combination of the two tracer methods provided unprecedented insights into structure-property relationships in severely deformed Ni. Abnormally high diffusion rates of Cr in ECAP-processed Ni are measured and the presence of a deformation-modified state of a fraction of the high-angle GBs is verified. For the first time, a co-existence of relaxed and deformation-modified high-angle GBs in ECAP Ni is unambiguously established addressing the different interfaces by correlative diffusion–microstructure investigation using different techniques on the same samples. The temperature/time evolution of the deformation-modified state of high-angle GBs is followed by dedicated measurements of the atomic transport and the microstructure characteristics.

The combination of the two complementary techniques allows a unique cross-scale characterization of the grain boundary diffusion properties spread over a large number of orders of magnitude in the same material. This approach occurred to be crucial for a rigorous analysis of the materials with an inherent multi-level hierarchy of diffusion properties of pertinent short-circuit-type defects.

Declaration of Competing Interest

The authors declare that they have no known competing financial interests or personal relationships that could have appeared to influence the work reported in this paper.

Acknowledgements

The authors are grateful to Prof. Y. Estrin and Dr. R. Lapovok (Monash University, Clayton, Australia) for fruitful collaboration and support in ECAP experiments. The funding by the French-German ANR-DFG DIPLOX project (DI 1419/16-1 and ANR-17-CE08-0049) is gratefully acknowledged.

References

[1] J.C. Fisher, Calculation of Diffusion Penetration Curves for Surface and Grain Boundary Diffusion, Journal of Applied Physics. 22 (1951) 74–77. https://doi.org/10.1063/1.1699825.
[2] A.D.L. Claire, The analysis of grain boundary diffusion measurements, British Journal of Applied Physics. 14 (1963) 351–356. https://doi.org/10.1088/0508-3443/14/6/317.
[3] R. Balluffi, Grain boundary diffusion mechanisms in metals, Metallurgical Transactions B. 13 (1982) 527–553.
[4] A. Paul, T. Laurila, V. Vuorinen, S.V. Divinski, Thermodynamics, diffusion and the Kirkendall effect in solids, Springer, 2014.

[5] Y. Mishin, C. Herzig, Grain boundary diffusion: recent progress and future research, Materials Science and Engineering: A. 260 (1999) 55–71. https://doi.org/10.1016/S0921-5093(98)00978-2.
[6] S. Divinski, M. Lohmann, C. Herzig, Grain Boundary Diffusion and Linear and Non-Linear Segregation of Ag in Cu, Interface Science. 11 (2003) 21–31. https://doi.org/10.1023/A:1021522620571.
[7] J. Čermák, Grain boundary self-diffusion of 51Cr and 59Fe in austenitic NiFeCr alloys, Materials Science and Engineering: A. 148 (1991) 279–287.
[8] J.M. Poate, K. Tu, J.W. Mayer, Thin films: interdiffusion and reactions, John Wiley & Sons, 1978.
[9] B. Burton, Diffusional Creep of Polycrystalline Materials. Trans. Tech. Publications, Bay Village OH, 1977.
[10] M.F. Ashby, A first report on deformation-mechanism maps, Acta Metallurgica. 20 (1972) 887–897.
[11] S. Divinski, G. Wilde, E. Rabkin, Y. Estrin, Ultra-Fast Atomic Transport in Severely Deformed Materials—A Pathway to Applications?, Advanced Engineering Materials. 12 (2010) 779–785. https://doi.org/10.1002/adem.200900340.
[12] T. Fujita, Z. Horita, T.G. Langdon, Characteristics of diffusion in Al-Mg alloys with ultrafine grain sizes, Philosophical Magazine A. 82 (2002) 2249–2262.
[13] Y.R. Kolobov, G. Grabovetskaya, K. Ivanov, M. Ivanov, Grain boundary diffusion and mechanisms of creep of nanostructured metals, Interface Science. 10 (2002) 31–36.
[14] H. Gleiter, Nanocrystalline Materials, in: W.G.J. Bunk (Ed.), Advanced Structural and Functional Materials, Springer Berlin Heidelberg, Berlin, Heidelberg, 1991: pp. 1–37.
[15] H. Gleiter, Proc. 2nd Riso Int. Symp. Metallurgy and Materials Science, (1981).
[16] R.Z. Valiev, R.K. Islamgaliev, I.V. Alexandrov, Bulk nanostructured materials from severe plastic deformation, Progress in Materials Science. 45 (2000) 103–189.
[17] J. Weertman, Hall-Petch strengthening in nanocrystalline metals, Materials Science and Engineering: A. 166 (1993) 161–167.
[18] C. Koch, Optimization of strength and ductility in nanocrystalline and ultrafine grained metals, Scripta Materialia. 49 (2003) 657–662.
[19] D. Morris, Mechanical Behaviour of Nanostructured Materials—Trans, Tech. Publ., Uetikon-Zurich. (1998).
[20] R.Z. Valiev, M.J. Zehetbauer, Y. Estrin, H.W. Höppel, Y. Ivanisenko, H. Hahn, G. Wilde, H.J. Roven, X. Sauvage, T.G. Langdon, The Innovation Potential of Bulk Nanostructured Materials, Advanced Engineering Materials. 9 (2007) 527–533. https://doi.org/10.1002/adem.200700078.
[21] W. Sprengel, R. Würschum, Diffusion in Nanocrystalline Metallic Materials, in: Bulk Nanostructured Materials, John Wiley & Sons, Ltd, 2009: pp. 501–517. https://doi.org/10.1002/9783527626892.ch23.
[22] M.J. Zehetbauer, Y. Estrin, Modeling of Strength and Strain Hardening of Bulk Nanostructured Materials, in: Bulk Nanostructured Materials, John Wiley & Sons, Ltd, 2009: pp. 109–136. https://doi.org/10.1002/9783527626892.ch5.
[23] M. Ames, J. Markmann, R. Karos, A. Michels, A. Tschöpe, R. Birringer, Unraveling the nature of room temperature grain growth in nanocrystalline materials, Acta Materialia. 56 (2008) 4255–4266. https://doi.org/10.1016/j.actamat.2008.04.051.
[24] G. Wilde, Nanostructured materials, Elsevier, 2009.
[25] R. Valiev, I. Alexandrov, Y. Zhu, T. Lowe, Paradox of strength and ductility in metals processed bysevere plastic deformation, Journal of Materials Research. 17 (2002) 5–8.
[26] R. Valiev, Nanomaterial advantage, Nature. 419 (2002) 887–889.
[27] Y. Wang, M. Chen, F. Zhou, E. Ma, High tensile ductility in a nanostructured metal, Nature. 419 (2002) 912–915.
[28] Y. Wang, E. Ma, Three strategies to achieve uniform tensile deformation in a nanostructured metal, Acta Materialia. 52 (2004) 1699–1709.
[29] J. Ribbe, G. Schmitz, H. Rösner, R. Lapovok, Y. Estrin, G. Wilde, S.V. Divinski, Effect of back pressure during equal-channel angular pressing on deformation-induced porosity in copper, Scripta Materialia. 68 (2013) 925–928. https://doi.org/10.1016/j.scriptamat.2013.02.034.

[30] J. Ribbe, D. Baither, G. Schmitz, S.V. Divinski, Network of porosity formed in ultrafine-grained copper produced by equal channel angular pressing, Physical Review Letters. 102 (2009) 165501.
[31] J. Ribbe, D. Baither, G. Schmitz, S.V. Divinski, Ultrafast diffusion and internal porosity in ultrafine-grained copper–lead alloy prepared by equal channel angular pressing, Scripta Materialia. 61 (2009) 129–132.
[32] S. Divinski, G. Reglitz, H. Rösner, Y. Estrin, G. Wilde, Self-diffusion in Ni prepared by severe plastic deformation: effect of non-equilibrium grain boundary state, Acta Mater. 59 (2011) 1974–1985.
[33] X. Sauvage, G. Wilde, S.V. Divinski, Z. Horita, R.Z. Valiev, Grain boundaries in ultrafine grained materials processed by severe plastic deformation and related phenomena, Materials Science and Engineering: A. 540 (2012) 1–12. https://doi.org/10.1016/j.msea.2012.01.080.
[34] A.A. Nazarov, A.E. Romanov, R.Z. Valiev, On the structure, stress fields and energy of nonequilibrium grain boundaries, Acta Metallurgica et Materialia. 41 (1993) 1033–1040. https://doi.org/10.1016/0956-7151(93)90152-I.
[35] R.C. Pond, D.A. Smith, On the absorption of dislocations by grain boundaries, The Philosophical Magazine: A Journal of Theoretical Experimental and Applied Physics. 36 (1977) 353–366. https://doi.org/10.1080/14786437708244939.
[36] R.A. Varin, Spreading of extrinsic grain boundary dislocations in austenitic steel, Physica Status Solidi (a). 52 (1979) 347–356. https://doi.org/10.1002/pssa.2210520139.
[37] R. Varin, K. Tangri, The effect of extrinsic grain boundary dislocations with unrelaxed and relaxed cores on the state of random boundaries in an austenitic steel, Metallurgical Transactions A. 12 (1981) 1859–1866.
[38] P.H. Pumphrey, H. Gleiter, On the structure of non-equilibrium high-angle grain boundaries, The Philosophical Magazine: A Journal of Theoretical Experimental and Applied Physics. 32 (1975) 881–885. https://doi.org/10.1080/14786437508221629.
[39] R.Z. Valiev, R.Sh. Musalimov, N.K. Tsenev, The non-equilibrium state of grain boundaries and the grain boundary precipitations in aluminium alloys, Physica Status Solidi (a). 115 (1989) 451–457. https://doi.org/10.1002/pssa.2211150211.
[40] A.M. Glaeser, J. Evans, Effect of grain boundary migration on apparent boundary diffusion coefficients, Acta Metallurgica. 34 (1986) 1545–1552.
[41] Y.R. Kolobov, G. Grabovetskaya, M. Ivanov, A. Zhilyaev, R. Valiev, Grain boundary diffusion characteristics of nanostructured nickel, Scripta Materialia. 44 (2001) 873–878.
[42] Y. Amouyal, S. Divinski, Y. Estrin, E. Rabkin, Short-circuit diffusion in an ultrafine-grained copper–zirconium alloy produced by equal channel angular pressing, Acta Materialia. 55 (2007) 5968–5979.
[43] G. Wilde, S. Divinski, Grain Boundaries and Diffusion Phenomena in Severely Deformed Materials, Materials Transactions. 60 (2019) 1302–1315. https://doi.org/10.2320/matertrans.MF201934.
[44] Y. Amouyal, S.V. Divinski, L. Klinger, E. Rabkin, Grain boundary diffusion and recrystallization in ultrafine grain copper produced by equal channel angular pressing, Acta Materialia. 56 (2008) 5500–5513. https://doi.org/10.1016/j.actamat.2008.07.029.
[45] L. Klinger, E. Rabkin, A model of grain boundary diffusion in polycrystals with evolving microstructure, International Journal of Materials Research. 100 (2009) 530–535. https://doi.org/10.3139/146.110068.
[46] D. Prokoshkina, L. Klinger, A. Moros, G. Wilde, E. Rabkin, S.V. Divinski, Effect of recrystallization on diffusion in ultrafine-grained Ni, Acta Materialia. 69 (2014) 314–325. https://doi.org/10.1016/j.actamat.2014.02.002.
[47] D. Prokoshkina, L. Klinger, A. Moros, G. Wilde, E. Rabkin, S.V. Divinski, Persistence of ultrafast atomic diffusion paths in recrystallizing ultrafine grained Ni, Scripta Materialia. 101 (2015) 91–94. https://doi.org/10.1016/j.scriptamat.2015.01.027.
[48] H. Mehrer, Diffusion in solids: fundamentals, methods, materials, diffusion-controlled processes, Springer Science & Business Media, 2007.
[49] D.D. Pruthi, M.S. Anand, R.P. Agarwala, Diffusion of chromium in Inconel-600, Journal of Nuclear Materials. 64 (1977) 206–210. https://doi.org/10.1016/0022-3115(77)90026-5.

[50] D. Treheux, P. Guiraldenq, Volume and Intergranular Diffusion of Iron, Chromium and Nickel in Inconel-Type Alloys, Mém. Sci. Rev. Métall. 78 (1981) 409.
[51] T.-F. Chen, G. Tiwari, Y. Iijima, K. Yamauchi, Volume and Grain Boundary Diffusion of Chromium in Ni-Base Ni-Cr-Fe Alloys, MATERIALS TRANSACTIONS. 44 (2003) 40–46. https://doi.org/10.2320/matertrans.44.40.
[52] P Guiraldenq P; Poyet, Etude comparative de la diffusion intergranulaire et de la desorption ulterieure du chrome vers la surface dans les alliages Ni75Cr16Fe9 (type INCONEL 600) en presence de vapeur d'eau par l'emploi du radiotraceur 51Cr, Mem. Etud. Sci. Rev. Metall.; Bibl. 20 Ref. 77 (1980) 939–949.
[53] P. Moulin, A.M. Huntz, P. Lacombe, Influence du carbone sur la diffusion du chrome et du nickel en volume et dans les joints de grains de l'alliage Ni-Cr 80/20, Acta Metallurgica. 27 (1979) 1431–1443. https://doi.org/10.1016/0001-6160(79)90165-2.
[54] B.-A. Chetroiu, Corrosion sous contrainte de l'alliage 600 en millieu primaire des REP: étude de la diffusion du chrome, PhD Thesis, Paris, ENMP, 2015.
[55] T. Gheno, F. Jomard, C. Desgranges, L. Martinelli, Tracer diffusion of Cr in Ni and Ni-22Cr studied by SIMS, Materialia. 3 (2018) 145–152. https://doi.org/10.1016/j.mtla.2018.08.004.
[56] D. Prokoshkina, V.A. Esin, G. Wilde, S.V. Divinski, Grain boundary width, energy and self-diffusion in nickel: Effect of material purity, Acta Materialia. 61 (2013) 5188–5197. https://doi.org/10.1016/j.actamat.2013.05.010.
[57] S.V. Divinski, G. Reglitz, M. Wegner, M. Peterlechner, G. Wilde, Effect of pinning by an orientation gradient on the thermal stability of ultrafine grained Ni produced by equal channel angular pressing, Journal of Applied Physics. 115 (2014) 113503. https://doi.org/10.1063/1.4867416.
[58] D. Gärtner, L. Belkacemi, V.A. Esin, F. Jomard, A.A. Fedotov, J. Schell, J.V. Osinskaya, A.V. Pokoev, C. Duhamel, A. Paul, S.V. Divinski, Techniques of Tracer Diffusion Measurements in Metals, Alloys and Compounds, Diffusion Foundations. 29 (2021) 31–73. https://doi.org/10.4028/www.scientific.net/DF.29.31.
[59] S.M. Daiser, C. Scholze, J.L. Maul, The checkerboard technique: An essential progress in SIMS data acquisition and evaluation, Nuclear Instruments and Methods in Physics Research Section B: Beam Interactions with Materials and Atoms. 35 (1988) 544–549. https://doi.org/10.1016/0168-583X(88)90328-X.
[60] P. Van der Heide, Secondary ion mass spectrometry: an introduction to principles and practices, John Wiley & Sons, 2014.
[61] B. Beausir, J. Fundenberger, Analysis Tools for Electron and X-ray diffraction, ATEX-Software, Www. Atex-Software. Eu, Université de Lorraine-Metz. (2017).
[62] O. Muránsky, L. Balogh, M. Tran, C.J. Hamelin, J.-S. Park, M.R. Daymond, On the measurement of dislocations and dislocation substructures using EBSD and HRSD techniques, Acta Materialia. 175 (2019) 297–313. https://doi.org/10.1016/j.actamat.2019.05.036.
[63] J.F. Nye, Some geometrical relations in dislocated crystals, Acta Metallurgica. 1 (1953) 153–162. https://doi.org/10.1016/0001-6160(53)90054-6.
[64] W. Pantleon, Resolving the geometrically necessary dislocation content by conventional electron backscattering diffraction, Scripta Materialia. 58 (2008) 994–997. https://doi.org/10.1016/j.scriptamat.2008.01.050.
[65] C.F. Gu, L.S. Tóth, B. Beausir, Modeling of large strain hardening during grain refinement, Scripta Materialia. 66 (2012) 250–253. https://doi.org/10.1016/j.scriptamat.2011.11.002.
[66] L. Harrison, Influence of dislocations on diffusion kinetics in solids with particular reference to the alkali halides, Transactions of the Faraday Society. 57 (1961) 1191–1199.
[67] T. Suzuoka, Lattice and Grain Boundary Diffusion in Polycrystals, Transactions of the Japan Institute of Metals. 2 (1961) 25–32. https://doi.org/10.2320/matertrans1960.2.25.
[68] I. Kaur, Y. Mishin, W. Gust, others, Fundamentals of grain and interphase boundary diffusion, John Wiley, 1995.
[69] S. Sevlikar G.M. Muralikrishna M. Vaidya V.A. Esin V. Razumovskii C. Duhamel S.V. Divinski, Unpublished. (2021).
[70] A.S. Ebner, S. Jakob, H. Clemens, R. Pippan, V. Maier-Kiener, S. He, W. Ecker, D. Scheiber, V.I. Razumovskiy, Grain boundary segregation in Ni-base alloys: A combined atom probe

tomography and first principles study, Acta Materialia. 221 (2021) 117354. https://doi.org/10.1016/j.actamat.2021.117354.
[71] S.V. Divinski, G. Reglitz, I.S. Golovin, M. Peterlechner, R. Lapovok, Y. Estrin, G. Wilde, Effect of heat treatment on diffusion, internal friction, microstructure and mechanical properties of ultra-fine-grained nickel severely deformed by equal-channel angular pressing, Acta Materialia. 82 (2015) 11–21. https://doi.org/10.1016/j.actamat.2014.08.064.
[72] D. Setman, E. Schafler, E. Korznikova, M.J. Zehetbauer, The presence and nature of vacancy type defects in nanometals detained by severe plastic deformation, Materials Science and Engineering: A. 493 (2008) 116–122. https://doi.org/10.1016/j.msea.2007.06.093.
[73] C. Moussa, M. Bernacki, R. Besnard, N. Bozzolo, Statistical analysis of dislocations and dislocation boundaries from EBSD data, Ultramicroscopy. 179 (2017) 63–72.
[74] J. Baton, W. Geslin, C. Moussa, Orientation and deformation conditions dependence of dislocation substructures in cold deformed pure tantalum, Materials Characterization. 171 (2021) 110789. https://doi.org/10.1016/j.matchar.2020.110789.
[75] A.M. Glaeser, J. Evans, Effect of grain boundary migration on apparent boundary diffusion coefficients, Acta Metallurgica. 34 (1986) 1545–1552.
[76] M. Hillert, G.R. Purdy, Chemically induced grain boundary migration, Acta Metallurgica. 26 (1978) 333–340. https://doi.org/10.1016/0001-6160(78)90132-3.
[77] J. Čermák, Diffusion Along Moving Grain Boundaries, Physica Status Solidi (a). 120 (1990) 351–361. https://doi.org/10.1002/pssa.2211200206.
[78] A. McCaig, S.J. Covey-Crump, W. Ben Ismaïl, G.E. Lloyd, Fast diffusion along mobile grain boundaries in calcite, Contributions to Mineralogy and Petrology. 153 (2007) 159–175. https://doi.org/10.1007/s00410-006-0138-8.
[79] P. Zięba, A. Paw\lowski, W. Gust, The role of grain boundary diffusion in discontinuous reactions, in: Defect and Diffusion Forum, Trans Tech Publ, 2001: pp. 1759–1766.
[80] G.A. López, P. Zięba, W. Gust, E.J. Mittemeijer, Analytical Electron Microscopy in a Discontinuous Precipitated Cu–In Alloy, Microchimica Acta. 145 (2004) 101–105.
[81] S.V. Divinski, M. Lohmann, T. Surholt, Chr. Herzig, Grain Boundary Motion during Ag and Cu Grain Boundary Diffusion in Cu Polycrystals, Interface Science. 9 (2001) 357–363. https://doi.org/10.1023/A:1015187501784.
[82] F. Guethoff, Yu. Mishin, C. Herzig, Self-diffusion along stationary and moving grain boundaries in α-Hf, Zeitschrift Fuer Metallkunde. 84 (1993) 584–591.
[83] G. Wilde, J. Ribbe, G. Reglitz, M. Wegner, H. Rösner, Y. Estrin, M. Zehetbauer, D. Setman, S. Divinski, Plasticity and Grain Boundary Diffusion at Small Grain Sizes, Advanced Engineering Materials. 12 (2010) 758–764. https://doi.org/10.1002/adem.200900333.
[84] S.V. Divinski, G. Reglitz, G. Wilde, Grain boundary self-diffusion in polycrystalline nickel of different purity levels, Acta Materialia. 58 (2010) 386–395. https://doi.org/10.1016/j.actamat.2009.09.015.
[85] T. Surholt, Chr. Herzig, Grain boundary self-diffusion in Cu polycrystals of different purity, Acta Materialia. 45 (1997) 3817–3823. https://doi.org/10.1016/S1359-6454(97)00037-2.
[86] Zs. Tôkei, Z. Erdélyi, Ch. Girardeaux, A. Rolland, Effect of sulphur content and pre-annealing treatments on nickel grain-boundary diffusion in high-purity copper, Null. 80 (2000) 1075–1083. https://doi.org/10.1080/01418610008212101.
[87] G. Reglitz, B. Oberdorfer, N. Fleischmann, J.A. Kotzurek, S.V. Divinski, W. Sprengel, G. Wilde, R. Würschum, Combined volumetric, energetic and microstructural defect analysis of ECAP-processed nickel, Acta Materialia. 103 (2016) 396–406. https://doi.org/10.1016/j.actamat.2015.10.004.
[88] D. Gupta, Influence of solute segregation on grain-boundary energy and self-diffusion, Metallurgical Transactions A. 8 (1977) 1431–1438.
[89] V. Borisov, V. Golikov, G. Scherbedinskiy, Relation between diffusion coefficients and grain boundary energy, Phys. Met. Metall. 17 (1964) 881–885.
[90] M. Shepelenko, L. Klinger, E. Rabkin, A. Berner, D. Prokoshkina, G. Reglitz, J. Fiebig, G. Wilde, S.V. Divinski, Recovery, recrystallization and diffusion in cold-rolled Ni, International Journal of Materials Research. 106 (2015) 554–564.

[91] P. Guiraldenq, Diffusion intergranulaire et energie des joints de grains [Grain boundary diffusion and energy], J. Phys. C. 36 (1975) 201–211.
[92] D. Gupta, Diffusion, Solute Segregations and Interfacial Energies in Some Material: An Overview, Interface Science. 11 (2003) 7–20. https://doi.org/10.1023/A:1021570503733.
[93] Z.B. Wang, K. Lu, G. Wilde, S.V. Divinski, Interfacial diffusion in Cu with a gradient nanostructured surface layer, Acta Materialia. 58 (2010) 2376–2386. https://doi.org/10.1016/j.actamat.2009.12.024.
[94] D.E. Page, K.F. Varela, O.K. Johnson, D.T. Fullwood, E.R. Homer, Measuring simulated hydrogen diffusion in symmetric tilt nickel grain boundaries and examining the relevance of the Borisov relationship for individual boundary diffusion, Acta Materialia. 212 (2021) 116882. https://doi.org/10.1016/j.actamat.2021.116882.
[95] B.S. Bokshtein, V.A. Esin, A.O. Rodin, A new model of grain-boundary segregation with the formation of atomic complexes in a grain boundary, The Physics of Metals and Metallography. 109 (2010) 316–322. https://doi.org/10.1134/S0031918X10040022.
[96] V.A. Esin, Y. Souhar, Solvent grain boundary diffusion in binary solid solutions: a new approach to evaluate solute grain boundary segregation, Philosophical Magazine. 94 (2014) 4066–4079. https://doi.org/10.1080/14786435.2014.980043.
[97] V.A. Esin, B.S. Bokstein, Effect of atomic interaction on grain boundary diffusion in the B regime, Acta Materialia. 60 (2012) 5109–5116. https://doi.org/10.1016/j.actamat.2012.06.011.
[98] J. Růžičková, B. Million, Self-diffusion of the components in the F.C.C. phase of binary solid solutions of the Fe-Ni-Cr system, Materials Science and Engineering. 50 (1981) 59–64. https://doi.org/10.1016/0025-5416(81)90086-0.
[99] M.A. Tschopp, S.P. Coleman, D.L. McDowell, Symmetric and asymmetric tilt grain boundary structure and energy in Cu and Al (and transferability to other fcc metals), Integrating Materials and Manufacturing Innovation. 4 (2015) 176–189. https://doi.org/10.1186/s40192-015-0040-1.
[100] S.R. K, S. Sankaran, K.C.H. Kumar, H. Rösner, M. Peterlechner, V.A. Esin, S. Divinski, G. Wilde, Grain boundary diffusion and grain boundary structures of a Ni-Cr-Fe- alloy: Evidences for grain boundary phase transitions, Acta Materialia. 195 (2020) 501–518. https://doi.org/10.1016/j.actamat.2020.05.051.

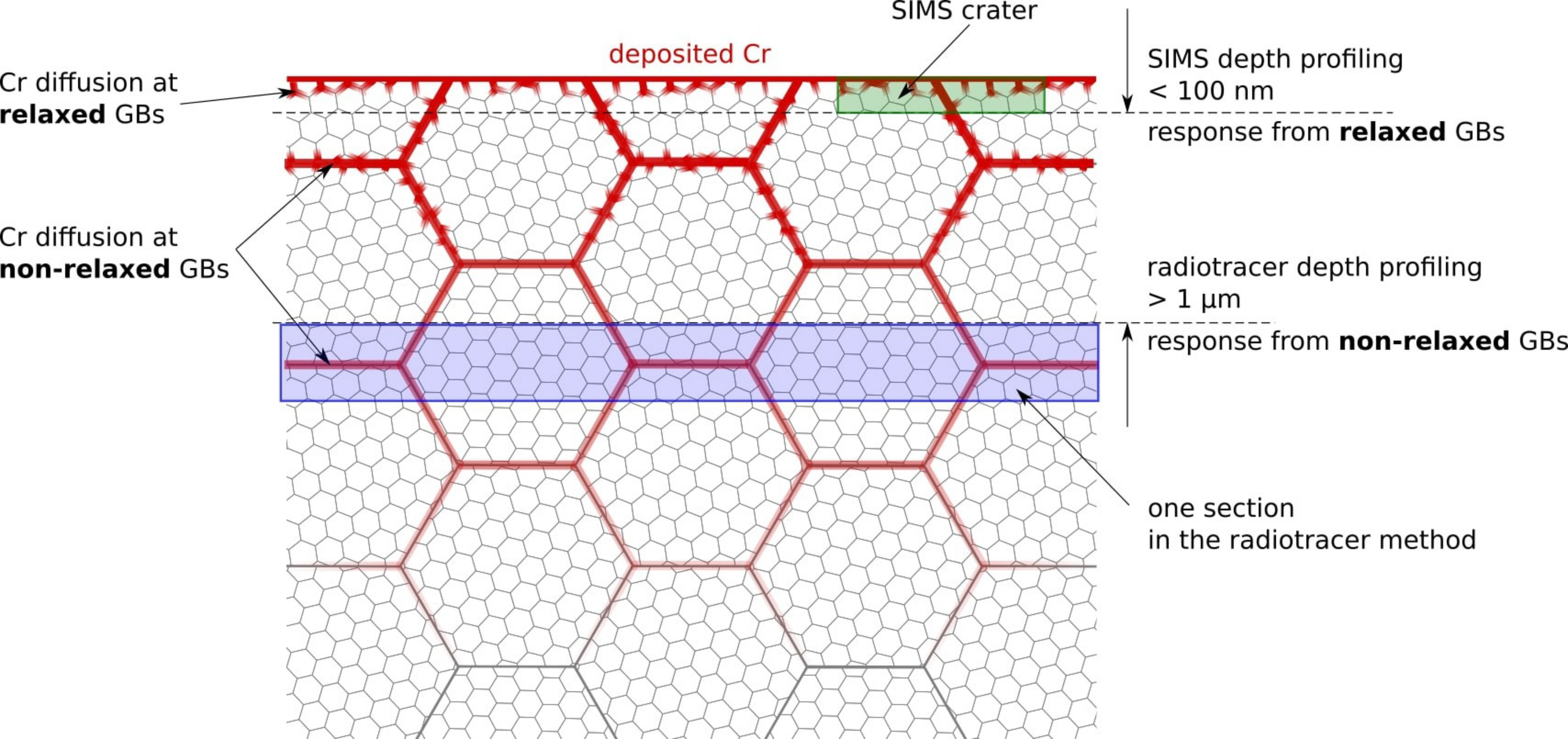
SIMS crater
deposited Cr
Cr diffusion at
relaxed GBs
Cr diffusion at
non-relaxed GBs
SIMS depth profiling
< 100 nm
response from **relaxed** GBs
radiotracer depth profiling
> 1 µm
response from **non-relaxed** GBs
one section
in the radiotracer method